High-resolution numerical simulations of resuspending gravity currents: Conditions for self-sustainment

F. Blanchette,[1,2] M. Strauss,[3] E. Meiburg,[1] B. Kneller,[4,5] and M. E. Glinsky[6]

Received 21 February 2005; revised 30 June 2005; accepted 29 August 2005; published 22 December 2005.

[1] We introduce a computational model for high-resolution simulations of particle-laden gravity currents. The features of the computational model are described in detail, and validation data are discussed. Physical results are presented that focus on the influence of particle entrainment from the underlying bed. As turbulent motions detach particles from the bottom surface, resuspended particles entrained over the entire length of the current are transferred to the current's head, causing it to become denser and potentially accelerating the front of the current. The conditions under which turbidity currents may become self-sustaining through particle entrainment are investigated as a function of slope angle, current and particle size, and particle concentration. The effect of computational domain size and initial aspect ratio of the current on the evolution of the current are also considered. Applications to flows traveling over a surface of varying slope angle, such as turbidity currents spreading down the continental slope, are modeled via a spatially varying gravity vector. Particular attention is given to the resulting particle deposits and erosion patterns.

Citation: Blanchette, F., M. Strauss, E. Meiburg, B. Kneller, and M. E. Glinksy (2005), High-resolution numerical simulations of resuspending gravity currents: Conditions for self-sustainment, *J. Geophys. Res.*, *110*, C12022, doi:10.1029/2005JC002927.

1. Introduction

[2] Gravity currents are flows generated when a predominantly horizontal density gradient is present in a fluid and hydrostatic pressure differences cause the heavy fluid to spread underneath the light fluid. In geophysical contexts, the density difference between the current and the ambient fluid is often due to the presence of suspended particles which act as the current's driving force. Such particles also settle relative to the fluid and may deposit at the bottom edge of the current. In particular, the dynamics of particle-laden gravity currents are relevant to ash-laden volcanic flows [*Sparks et al.*, 1991], crystal laden flows in magma chambers [*Hodson*, 1998] and turbidity currents, i.e., underwater currents in which the excess density is provided by suspended sediment [*Simpson*, 1997].

[3] Erosion by turbidity currents is largely responsible for the creation of submarine canyons on continental slopes [e.g., *Pratson and Coakley*, 1996]. Turbidity currents are the most significant agents of sediment transport into the deep sea, creating accumulations that include the Earth's largest sediment bodies [*Normark et al.*, 1993]. They also constitute a hazard to marine engineering installations such as oil platforms, pipelines and submarine cables [*Krause et al.*, 1970]. Natural turbidity currents occur infrequently and unpredictably in remote and hostile environments, and tend to be destructive of submarine monitoring equipment [e.g., *Zeng et al.*, 1991]. Consequently they are observed only rarely and generally by indirect means only [*Hay et al.*, 1982; *Hughes-Clarke et al.*, 1990]. Laboratory and numerical experiments thus constitute essential means of investigating these important large scale natural phenomena.

[4] Particle-laden gravity currents have been studied intensively in the past four decades. Turbidity currents are nonconservative in that they entrain ambient fluid through turbulent mixing, and deposit sediment as turbulent motions decay. They may also erode sediment from the bed, thus producing self-sustaining ("autosuspending" or "ignitive") currents [*Parker et al.*, 1986; *Pantin*, 1991, 2001]. Simplified analytical models have been suggested to describe density currents [*Huppert and Simpson*, 1980] and the asymptotic limit of small particle concentration was considered by using density-driven gravity currents as a known background flow [*Hogg et al.*, 2000]. Experimental studies of the progression of particle-laden currents with finite

[1]Department of Mechanical and Environmental Engineering, University of California, Santa Barbara, California, USA.
[2]Now at Department of Physics, University of Chicago, Chicago, Illinois, USA.
[3]Physics Department, Nuclear Research Center, Negev, Beer Sheva, Israel.
[4]Institute for Crustal Studies, University of California, Santa Barbara, California, USA.
[5]Now at Department of Geology, University of Aberdeen, Aberdeen, Scotland.
[6]BHP Billiton Petroleum, Houston, Texas, USA.

0148-0227/05/2005JC002927$09.00

volume [*Bonnecaze et al.*, 1993] or constant flux [*García and Parker*, 1993] were performed, and particular attention was given to the resulting deposits. Layer-averaged numerical models have been suggested by *Bonnecaze et al.* [1993] and *García and Parker* [1993]. Such simplified models require a number of closure assumptions regarding bottom friction, bottom shear stress, fluid entrainment and front velocity. More recently, highly resolved two-dimensional (2-D) and three-dimensional (3-D) simulations computing fluid flow from first principles have successfully described particle-laden gravity currents [*Necker et al.*, 2002]. Several features of the flow, such as energy and particle concentration distribution may easily be computed from these simulations and significantly fewer closure assumptions are required in such models. For those reasons, a similar approach is used in the present study to model resuspending gravity currents.

[5] The geometry of the surface over which currents propagate determines their long term behavior. For density currents, experimental studies of the influence of the slope angle were performed by *Britter and Linden* [1980] and *Beghin et al.* [1981]. Particle-laden currents traveling down a broken slope were investigated by *García* [1993] owing to their relevance to turbidity currents spreading down the continental shelf before reaching a relatively flat ocean bottom. Complex geometries were recently included in highly resolved simulations via the inclusion of a spatially varying gravity vector in a rectangular computational domain [*Blanchette et al.*, 2005]. If a current is spreading over an erodible bed, the geometry of the base may allow the current to resuspend sufficient particles so that its mass and velocity increase as it progresses down slope. This phenomenon is responsible for the destructive power of avalanches [*Hutter*, 1996]. Self-sustaining turbidity currents are known to occur in the oceans where they may travel over hundreds of kilometers, as exemplified by the Grand Banks turbidity current of 1929 [*Heezen and Ewing*, 1952].

[6] The flux of resuspended particles as a function of flow and particle parameters is particularly difficult to estimate. Several empirical models have been suggested [*Smith and McLean*, 1977; *García and Parker*, 1991, 1993], but their applicability remains limited and they must be used with caution. Direct numerical simulations have been employed to study the lift-off of particles in plane Poiseuille flow [*Choi and Joseph*, 2001], but such simulations are so far limited to a fairly small number of particles arranged in regular patterns [*Patankar et al.*, 2001]. At present, it is fair to say that a complete understanding of resuspension from an irregular bed of particles has not yet been achieved. However, because re-entrainment of particles is critical in the long-term behavior of gravity currents, it must be taken into account despite the limitations inherent in empirical models derived from experimental measurements.

[7] Our current study focuses on extending our earlier high-resolution simulations of nonresuspending turbidity currents [*Necker et al.*, 2002] to situations where resuspension is significant in order to investigate the depositional and erosional properties of such currents. Particular attention will be given to the conditions required for a particle-laden current to exhibit a snow ball effect. Specifically, we ask under which conditions a current becomes self-sustaining depending on parameters such as particle size and concentration, current height and slope angle. Our model and numerical approach are presented in section 2. We describe our results in section 3, and the implications of our findings are discussed in section 4.

2. Model Description

2.1. Governing Equations and Relevant Parameters

[8] We consider currents in which the particle concentration is relatively low, so that particle-particle interactions may be neglected. The density difference between the current and the ambient is thus typically small and we may use the Boussinesq approximation [e.g., *Spiegel and Veronis*, 1960], where density variations appear only in the buoyancy term. We use a continuum approach, where the density of the suspension, $\bar{\rho}$, is related to the particle concentration by volume, $\bar{C}$, through $\bar{\rho} = \bar{\rho}_f + \bar{C}(\bar{\rho}_p - \bar{\rho}_f)$, where $\bar{\rho}_f$ and $\bar{\rho}_p$ are the fluid and particle density, respectively, and the bars indicate dimensional (and nonnormalized) quantities. Particles are assumed to be transported by the fluid and to settle relative to the fluid with velocity $\bar{u}_s$ in the direction of gravity.

[9] The work by *Necker et al.* [2002] comparing 2-D and 3-D simulations of gravity currents showed that, even though vortices tend to be more vigorous in 2-D simulations than in full 3-D simulations, 2-D and 3-D simulations yield very similar results regarding the front propagation velocity and the spanwise averaged deposit profile. For this reason, we restrict our attention to 2-D systems. We eliminate pressure terms by considering a stream function-vorticity description of the fluid motion. Denoting the coordinate parallel to the bottom surface by x_1, that perpendicular by x_2 and the corresponding velocities by u_1 and u_2 respectively (see Figure 1), we introduce a stream function ψ satisfying $u_1 = \partial\psi/\partial x_2$ and $u_2 = -\partial\psi/\partial x_1$ and a vorticity function $\omega = \partial u_2/\partial x_1 - \partial u_1/\partial x_2$.

[10] We use the initial half-height of the suspension reservoir, $\bar{h}$, as a length scale, and the initial particle concentration, $\bar{C}_0$, as a concentration scale. As a typical velocity, we consider the buoyancy velocity

$$\bar{u}_b = \left(g\bar{h}\bar{C}_0 R\right)^{1/2}, \tag{1}$$

where g is the gravitational acceleration and $R = (\bar{\rho}_p - \bar{\rho}_f)/\bar{\rho}_f$. We thus obtain the following nondimensional governing equations [*Necker et al.*, 2002]

$$\nabla^2\psi = -\omega \tag{2}$$

$$\frac{D\omega}{Dt} = \frac{\nabla^2\omega}{Re} - \frac{\partial(C\cos\theta)}{\partial x_1} - \frac{\partial(C\sin\theta)}{\partial x_2} \tag{3}$$

$$\frac{DC}{Dt} + U_s\left(\frac{\partial(C\sin\theta)}{\partial x_1} - \frac{\partial(C\cos\theta)}{\partial x_2}\right) = \frac{\nabla^2 C}{Pe} \tag{4}$$

where we use the notation $D/Dt = \partial/\partial t + u_1\partial/\partial x_1 + u_2\,\partial/\partial x_2$ and where $U_s = \bar{U}_s/\bar{u}_b$, $Re = \bar{u}_b\,\bar{h}/\bar{\nu}$ is the Reynolds number and $Pe = \bar{u}_b\bar{h}/\bar{\kappa}$ the Péclet number, with $\bar{\nu}$ the fluid viscosity and $\bar{\kappa}$ the particle diffusion constant. Note that the

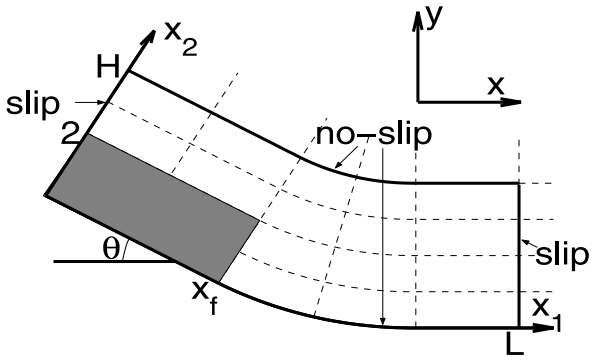

Figure 1. Schematic of the coordinate system used in our simulations. The angle θ between the x_1 axis and the horizontal axis is allowed to vary with x_1 to model varying slopes. The dark region corresponds to the initial position of the heavy fluid and is constrained by $0 \le x_1 \le x_f$, $0 \le x_2 \le 2$. The height and length of the computational domain are H and L, respectively.

only driving force of the flow comes from horizontal variations of C, i.e., variations along the x axis.

[11] It should be pointed out that, in principle, one can account for the force exerted by the particles onto the fluid in two different ways. In the first approach one considers the conservation equations for the suspension, i.e., the combined fluid/particle system. In this case, only external forces acting on the suspension should be considered, such as the action of the buoyancy force on the density field of the suspension. Internal forces acting within the suspension, such as the drag force between fluid and particles, are not considered separately in this case. This approach was taken by *Necker et al.* [2002], and is also pursued here. Alternatively, one may consider the fluid and the particles separately. In this case, the conservation equation for the constant density fluid contains a term that accounts for the drag force exerted by the particles on the fluid, but a separate buoyancy force does not appear in the equation. In that sense the drag force and the buoyancy force are equivalent to each other. This second approach was taken, for example, by *Bosse et al.* [2005].

[12] Our simulations aim at reproducing as closely as possible the physical conditions prevailing in large turbidity currents. We therefore elected to simulate currents in which water is the suspending fluid, i.e., $\bar{\rho}_f = 1\text{g/cm}^3$ and $\bar{\nu} = 10^{-6}\,\text{m}^2/\text{s}$. We consider particles of density $\bar{\rho}_p = 2.5\text{g/cm}^3$ ($R = 1.5$) and typical diameter $\bar{d} = 100\ \mu\text{m}$, values appropriate for sandy turbidity currents such as those forming many submarine fans [*Normark et al.*, 1993]. To compute the particle settling speed we employ the empirical formula of *Dietrich* [1982], $\bar{U}_s = (WgR\,\bar{\nu})^{1/3}$, where

$$W = 1.71 \times 10^{-4}\left(\frac{gR\bar{d}^3}{\bar{\nu}^2}\right)^2, \text{ if } \lambda < -1.3$$
$$= 10^{p(\lambda)}, \text{ otherwise,}$$

with $\lambda = \log_{10}(gR\ \bar{d}^3/\bar{\nu}^2)$ and $p(\lambda) = (-3.76715 + 1.92944\lambda - 0.09815\lambda^2 - 0.0057\lambda^3 + 0.00056\lambda^4)$. To compute the buoyancy velocity, we use a typical particle concentration of $\bar{C}_0 = 0.5\%$ and height of approximately $\bar{h} = 1.6$ m, which results in a nondimensional particle settling speed of $U_s = 0.02$.

[13] The above parameters correspond to a current Reynolds number of order 10^6, which is well beyond the current reach of direct numerical simulations. As Re increases, smaller length scales must be resolved, which in turn implies shorter time steps. However, as will be seen below in sections 3.1 and 3.2, provided $Re > O(1{,}000)$, variations in Re only have a small effect on the overall features of the flow, [cf. *Parsons and García*, 1998]. For this reason, most of the simulations to be discussed below will be carried out with a reduced Reynolds number $Re_T \ll Re$ which is kept in the range $1{,}000 < Re_T < 10{,}000$. This reduced Reynolds number can be interpreted as a simple way to model the effects of small-scale, unresolved flow structures. Our focus in the current investigation is on small particles with negligible inertia, whose velocity is given by the fluid velocity and a superimposed settling velocity. Hence it is reasonable to assume that the small-scale, unresolved flow structures will affect the transport of particles in the same way as the transport of fluid [*Shraiman and Siggia*, 2000], so that we set the value of the reduced Péclet number Pe_T equal to that of the reduced Reynolds number. Note that all other dimensionless parameters are kept at their original values for the typical turbidity current described above. We wish to remark that, while turbulence models have been developed for variable density [*Speziale*, 1991; *Choi and García*, 2002] and particle-laden flows [*Elghobashi and Abouarab*, 1983; *Hagatun and Eidsvik*, 1986; *Zhang and Reese*, 2001; *Hsu et al.*, 2003, and others], to the best of our knowledge there are no models that can accurately capture the complex physics in the nondilute layer next to a resuspending particle bed.

[14] We use a lock-release model, where heavy fluid is initially confined to a small region, $0 \le x_1 \le x_f$ and $0 \le x_2 \le 2$. The initial length of the current, x_f, may be varied but was usually kept at $x_f = 2$. For reasons of numerical stability, the initial concentration profile was smoothed over a few grid points (typically 6) using an error function centered at $x_1 = x_f$ in the horizontal and at $x_2 = 2$ in the vertical. The fluid is initially at rest, $\psi = \omega = 0$ and starts moving at $t = 0$.

[15] In order to model complex geometries, we use a spatially varying gravity vector [*Blanchette et al.*, 2005]. A curvilinear coordinate system is thus simulated but second-order curvature terms are neglected. The resulting approximation is expected to be valid if the ratio of the height of the flow to the radius of curvature of the bottom surface is everywhere small. We restrict our study to smoothly varying bottom surfaces to ensure that the neglected curvature effects remain small. We use a rectangular computational domain and enforce a no-slip, no normal flow condition at the top and bottom boundaries, $\psi = \partial\psi/\partial x_2 = 0$, and a slip, no normal flow condition at the left and right walls, $\psi = \partial^2\psi/\partial x_1^2 = 0$. The latter conditions allow for the use of fast Fourier transforms in the x_1 direction which provide high accuracy to our numerical scheme.

[16] The particle concentration flux at the boundaries, F, is set to zero at the top and left walls. At the right wall, which effectively is never reached by the heavy current, particles may deposit, but no resuspension is allowed so that $F = -CU_s \sin\theta$. However, particles are allowed to deposit and reenter suspension at the bottom boundary: $F = (-CU_s \cos\theta$

$+ E_s U_s$), where E_s is a measure of the resuspension flux as discussed below. Thus at the top and left boundaries the diffusive flux is equal to the settling flux, it is zero at the right wall and it is equal to the resuspension flux at the bottom surface:

$$CU_s \cos\theta + \frac{1}{Pe_T}\frac{\partial C}{\partial x_2} = 0 \quad \text{at } x_2 = H, \tag{5}$$

$$-CU_s \sin\theta + \frac{1}{Pe_T}\frac{\partial C}{\partial x_1} = 0 \quad \text{at } x_1 = 0, \tag{6}$$

$$\frac{\partial C}{\partial x_1} = 0 \quad \text{at } x_1 = L, \tag{7}$$

$$\frac{\partial C}{\partial x_2} = -Pe_T U_s E_s \qquad \text{at } x_2 = 0. \tag{8}$$

[17] Unresolved turbulent motions are assumed to be responsible for resuspending particles near the bottom boundary. The influx of particles due to resuspension is therefore modeled as a turbulent diffusive flux, as small scale turbulent motions bring deposited particles into the suspension. As compared to the frequently employed strategy of distributing the added particles equally over the entire height of the current, this diffusive flux approach represents a more realistic approximation of the physically complex resuspension process. The height of the deposit, $d(x_1, t)$, may be found by integrating the particle flux over time

$$d(x_1, t) = \frac{\bar{C}_0}{\sigma}\int_0^t \left(CU_s \cos\theta|_{x_2=0} - E_s U_s\right) dt,$$

where σ is the particle volume fraction in the bed, taken to be a constant $\sigma = 0.63$ [*Torquato et al.*, 2000]. Note that the corresponding porosity of the deposit is $1 - \sigma = 0.37$. Note that we consider only flows where $\bar{C}_0 \sim 1\%$ so that the erosion or deposition depth is small relative to the current size ($d \ll H$), which allows us to keep the position of the bottom boundary fixed in our computations.

[18] To evaluate the resuspension flux, $E_s U_s$, we use the empirical formula derived by *García and Parker* [1993] for turbidity current experiments, which relates the resuspension flux to the particle Reynolds number and bottom shear velocity. We consider an erodible bed composed of particles identical to those in suspension. A measure of the vigor of the resuspension is given by Z, which, following *García and Parker* [1993], is defined as

$$Z = \frac{u^*}{U_s} Re_p^{0.6} \qquad \text{if } Re_p > 2.36,$$

$$Z = 0.586\frac{u^*}{U_s} Re_p^{1.23} \qquad \text{if } Re_p \le 2.36$$

where u^* is the shear velocity at the bottom wall and Re_p is the particle Reynolds number

$$u^* = \left(\frac{1}{Re_T}\frac{\partial u}{\partial x_2}\bigg|_{x_2=0}\right)^{1/2}, \quad Re_p = \frac{\bar{d}\left(g\bar{d}R\right)^{1/2}}{\bar{\nu}}. \tag{9}$$

The lower and upper branches of Z reflect the different settling dynamics of low and high particle Reynolds numbers, respectively. The resuspension flux, $E_s U_s$, is then a threshold function of Z,

$$E_s = \frac{1}{\bar{C}_0}\frac{aZ^5}{1 + \frac{a}{0.3}Z^5}, \tag{10}$$

with $a = 1.3 \times 10^{-7}$. Notice that the normalization of E_s by the initial particle concentration renders the effect of resuspension more significant for dilute suspensions. Also, E_s may not exceed $0.3/\bar{C}_0$, thus providing a saturation mechanism.

[19] Modeling resuspension as a turbulent diffusive flux has the inconvenience of injecting energy into the current through particle diffusion: particles are lifted upward by diffusive effects without a corresponding energy loss. For small inclination angles and particle settling speed, ($\theta \le 2°$, $U_s \le 0.005$), this diffusive energy input may significantly affect the dynamics of the flow. For flat surfaces and small particle settling speeds, a more detailed description of the turbulence, such as that provided by a $K - \epsilon$ model [*Speziale*, 1991], may help to account for this energy input by decreasing the turbulent kinetic energy and shall be investigated in the future. However, for larger slope angles, the potential energy lost or gained by the current through the deposition or resuspension of particles located higher than the downstream bottom boundary is much larger than that gained through particle diffusion. The dynamics of the flow are therefore dominated by the potential energy of deposited or resuspended particles and our model is expected to adequately describe currents evolving over sufficiently large slopes. Similarly, for large settling speeds, the energy lost through particle settling is dominant and our approach is expected to correctly capture the main features of the flow.

2.2. Numerical Approach

[20] The numerical integration of equations (2)–(4) is performed in a manner similar to that of *Härtel et al.* [2000]. We perform a Fourier transform for ψ in the x_1 direction and use sixth-order compact finite differences for other derivatives, except near the boundaries where the derivatives are accurate to third order [*Lele*, 1992]. A third-order Runge-Kutta integrator is used to march equations (3)–(4) forward in time [*Härtel et al.*, 2000]. The velocity field is obtained by differentiating ψ. We use an adaptive time step to satisfy the Courant-Friedrichs-Levy and diffusive stability criteria while minimizing computation time. We solve the governing equations over a rectangular domain described by $0 \le x_1 \le L$, $0 \le x_2 \le H$, with typical values $L = 24$ and $H = 4$ and a grid of size 1025×385, which has been shown to be a sufficient resolution [*Blanchette et al.*, 2005]. The flow is found to be unaffected by the choice of L as long as the tip of the current remains more than one nondimensional unit away from the right wall. We investigate the influence of H in the following section.

[21] Large concentration derivatives near the bottom boundary may result from the modeling of resuspension as a diffusive flux. A finer grid is thus required near the bed than in other areas of the computational domain. To accelerate computations, we have implemented an unevenly spaced grid in the x_2 direction. By considering a Taylor

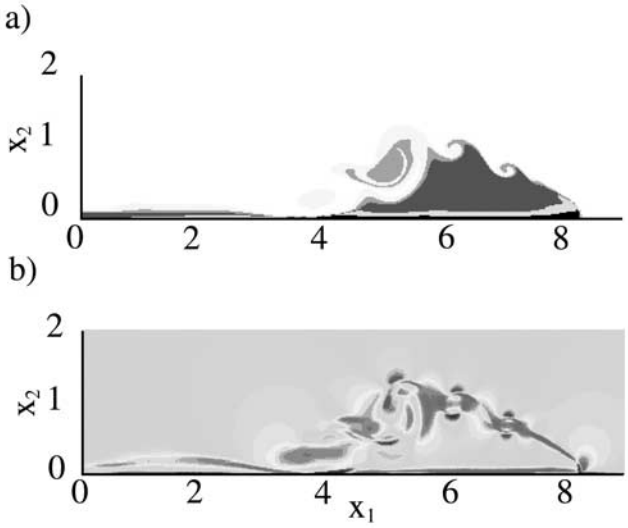

Figure 2. Sample of (a) the concentration and (b) vorticity of a particle-driven current traveling over a surface with an inclination angle $\theta = 5°$, at $t = 7.5$ computed via our numerical model. In Figure 2a the color code is: $0.1 < C \leq 0.5$ yellow, $0.5 < C \leq 0.8$ green, $0.8 < C \leq 1$ red, $1 < C \leq 3$ cyan, and $3 < C$ black. In Figure 2b, positive (counterclockwise), zero, and negative (clockwise) vorticity are shown in red, green, and blue, respectively. The simulation parameters are $H = 4$, $L = 24$, $x_f = 2$, $U_s = 0.02$, $Re_p = 3.83$, and $Re_T = Pe_T = 2{,}200$. See color version of this figure at back of this issue.

series expansion, we generalized the compact finite differences formulas presented in the work of *Lele* [1992] to allow for the use of a varying Δx_2. An example of the resulting formula used to compute a first derivative is shown in Appendix A. The obtained formulas are sixth-order accurate and their local error scales as the sixth power of the local Δx_2. To determine the position of the grid points, x_2^j, we evenly space grid points on a stretching variable $0 \leq s^j \leq 1$ and use a mapping function of the form [*Fletcher*, 1991]

$$x_2^j = H \frac{\tanh(\alpha(s^j - 1)) + \beta s^j + \tanh(\alpha)}{\tanh(\alpha) + \beta}$$

where typical values of the coefficients are $\alpha = 3$ and $\beta = 0.32$. These values yield $\Delta x_2 = 0.0028$ and $\Delta x_2 = 0.026$ near the bottom and top wall, respectively, with a continuous variation in the central region. Validation information will be provided as part of the next section.

3. Simulation Results

[22] We show in Figure 2 typical concentration and vorticity fields associated with a particle-driven current computed via the model presented in section 2. Here the current is traveling over a surface with a relatively large slope angle, $\theta = 5°$, and is therefore predominantly erosional. Resuspension increases the particle concentration near the bottom boundary (blue and black zones) to a level exceeding the initial concentration $C = 1$. Vortices are shed behind the head of the current and form nearly circular regions of nonzero particle concentration (yellow and green in Figure 2a) embedded in ambient fluid. Such vortices generate mixing with ambient fluid, causing the particle concentration to decrease below its initial value. They are also responsible for a significant fraction of the viscous energy dissipation and therefore act to reduce the kinetic energy of the current. The largest vorticity is found near the bottom boundary due to the no-slip boundary condition. The bottom shear stress is sufficiently large to cause particles to be re-entrained. Behind the head of the current, vortices are seen to vertically mix the particle concentration. Fluid in the rear of the current tends to catch up with the front [*Härtel et al.*, 2000], causing high particle concentrations to develop near the head.

3.1. Influence of the Reduced Reynolds and Péclet Numbers

[23] We begin by studying the impact of the reduced Reynolds number used in our simulations on the main features of the flow. Figure 3 shows the time evolution of the position of the front of a density current ($U_s = 0$) traveling over a horizontal surface. For relatively small reduced Reynolds numbers, $Re_T < 1{,}000$, the front velocity increases significantly with Re_T. However this dependence becomes negligible for larger reduced Reynolds numbers. For sufficiently large values of Re_T, other qualitative features of the flow, such as the shape and number of vortices shed behind the head or the size of the head, were also observed to be nearly independent of Re_T, which validates the use of a reduced Reynolds number, provided $Re_T > 1{,}000$.

[24] The value of Re_T only has a week influence on our resuspension model. The nondimensional bottom shear velocity near a solid wall, u^*, is known to de-

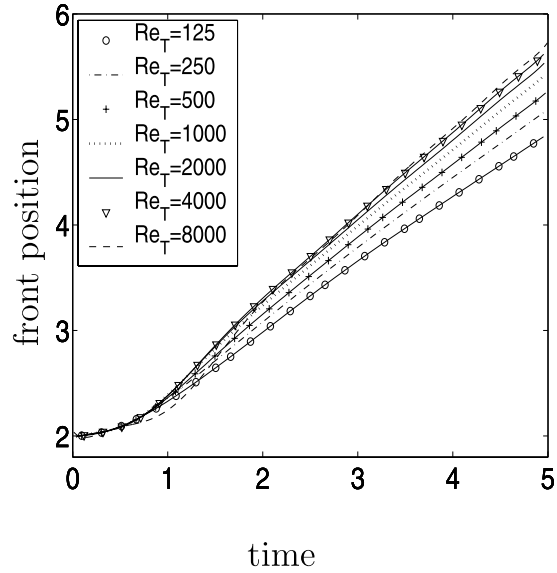

Figure 3. Time-dependence of the front position of a density current ($U_s = 0$) traveling over a horizontal surface for various values of the reduced Reynolds number. For $Re_T \geq O(1{,}000)$ the front velocity becomes nearly independent of Re_T. Other parameters are $x_f = 2$, $H = 4$, $L = 12$, and $Pe_T = Re_T$.

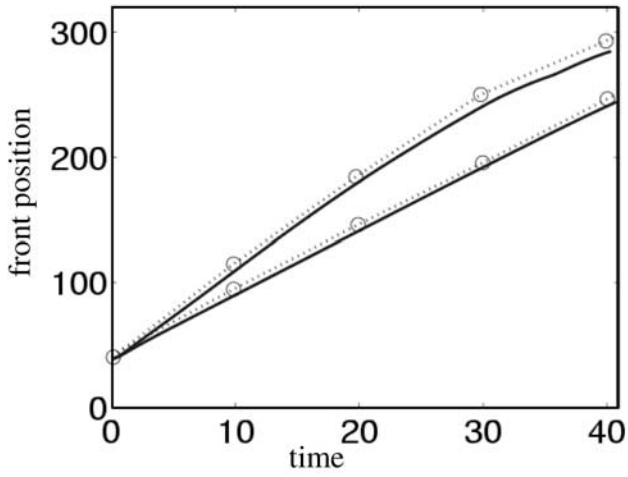

Figure 4. Comparison of the position of the front of a density current as a function of time measured experimentally by *Huppert and Simpson* [1980] (circles) with that computed via our simulations (solid line). In nondimensional form the parameters used are: $H = 5.87$, $C_0 = 0.0096$, $x_f = 5.21$, and $Re = 6300$, and experiments are nondimensionalized using typical length and time $L = 7.5$ cm and $t = 0.89$ s. There are no free parameters in the simulations.

crease logarithmically with increasing Reynolds number [*Barenblatt*, 1993], which tends to reduce resuspension for large values of Re_T. This may be understood by noting in equation (9) that $u^* \sim 1/Re_T$ so that even though larger Re_T generate larger $\partial u/\partial x_2$, the net effect of increasing the Reynolds number is to decrease u^*. However, because of the logarithmic dependence of u^* on Re_T, little effect was observed in our simulations. The above resuspension model also depends on Pe_T, as particles resuspended from the bed are distributed over a layer of thickness $\delta_r \sim Pe_T^{-1/2}$. The influence on resuspension of Pe_T is analogous to that of the ratio, r_0, of the particle concentration near the bed to the average concentration in the current of layer averaged models [*Parker et al.*, 1987]. A suitable value of Pe_T can be determined from experimental measurements of r_0. Data provided by *García* [1994] suggest that $r_0 = 2$, which is approximately reproduced in our simulations for $Pe_T = 2{,}200$, a value which will be used in the remainder of this paper. Further comparisons between our simulations and experiments are discussed in the next section.

[25] It should be noted that quantitatively similar results were obtained from a cruder resuspension model. In preliminary simulations, the diffusive flux at the bottom boundary was set to zero, and resuspended particles were simply added uniformly over a layer of uniform thickness, $\delta_r \approx 0.1$, near the bottom boundary. The added mass of resuspended particles was computed at every time step, $M_r(x_1) = E_s U_s \Delta t$, and the concentration was increased in the resuspension layer

$$C(x_1, x_2, t) = C'(x_1, x_2, t) + M_r/\delta_r, \qquad \text{if } 0 < x_2 < \delta_r$$

where C' was obtained by advancing in time equations (2)–(4). The general features of the flow agreed well with those observed when particles are resuspended through a diffusive flux. The dependence on Re_T was similar in both models and increasing δ_r was analogous to reducing Pe_T. Keeping in mind that even the strategy of distributing resuspended particles over the entire current height has been successfully used in layer averaged models [cf. *García*, 1994], it can be hence be concluded that the dominant features of the flow, and in particular whether or not a flow is self-sustaining, are largely independent of the details of the resuspension model.

3.2. Comparison With Experiments

[26] We present in this section a comparison between our numerical simulations and experimental data published in the literature. We first show in Figure 4 the measured length of a density current ($U_s = 0$) as a function of time and compare it to our simulations. The experimental results displayed here were obtained by *Huppert and Simpson* [1980] and we used corresponding governing parameters in our simulations, $Re = 6300$. In particular, the nondimensional height of the container is $H = 5.87$, which ensures that the influence of the top surface on the propagation of the current is minimal. The time-dependent position of the front, and consequently the speed of density current, is seen to be accurately reproduced by the simulation. Experiment and simulation are seen to agree well for more than 30 nondimensional time units, by which time the current has lost most of its structure. This comparison demonstrates the ability of the simulations to reproduce the front velocity.

[27] We proceed with a comparison of the progression of particle-laden currents. In this context, experiments are constrained by the necessity to maintain particles in suspension before the lock is released. Therefore they are usually performed in a shallow ambient, and with a free

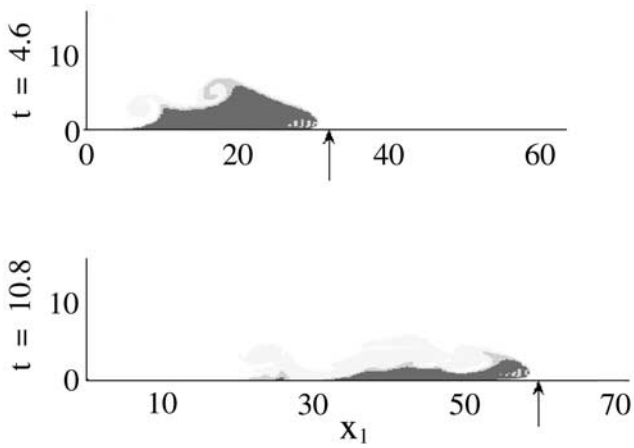

Figure 5. Progression of a particle-laden current with governing parameters identical to those of the current shown in the work of *Bonnecaze et al.* [1993, Figure 9a]. The arrows indicate the position of the front recorded in the experiment. In nondimensional form the parameters used are: $H = 2$, $U_s = 0.03$, $x_f = 1.14$, and $Re_p = 1.8$, and experiments are nondimensionalized using typical length and time $L = 7$ cm and $t = 0.64$ s. The experimental Reynolds number is $Re = 7600$; simulations were performed with a reduced value $Re_T = 2200$. See color version of this figure at back of this issue.

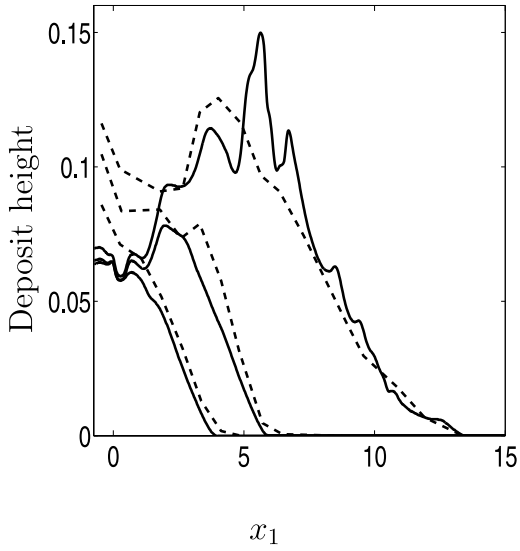

Figure 6. Comparison of the normalized deposit height (the total volume of the deposit is set to one) obtained experimentally by *De Rooij and Dalziel* [2001] (dashed line) with that obtained via our simulations (solid line). In nondimensional form the parameters used are: $H = 2$, $U_s = 0.02$, $x_f = 0.75$, and $Re_p = 1.05$, and experiments are nondimensionalized using typical length and time $L = 13.25$ cm and $t = 1.64$ s. The experimental Reynolds number is $Re = 10{,}000$; simulations were performed with a reduced value $Re_T = 2{,}200$.

surface. The fact that we model the top surface as a no-slip wall rather than a free surface is then expected to cause more substantial discrepancies between experiments and simulations because our simulations cannot capture the vertical displacement of the top surface. We show in Figure 5 simulations computed for identical parameter values as in the experiments of *Bonnecaze et al.* [1993, Figure 9a]. Here the concentration of a particle-laden current is shown at two different times. The arrows indicate the front position recorded in the experiment at corresponding times. The experiments show some 3-D turbulence and were performed at higher Reynolds number ($\approx$7,600) than our simulations ($Re_T = 2{,}200$). Nevertheless, the concentration field shown in Figure 5 exhibits good agreement with the experiments, which further justifies the use of a reduced Reynolds number value. In particular, the general shape, length, and consequently velocity, of the current are rather well reproduced. The bore described by *Bonnecaze et al.* [1993] due to the reflection of light fluid off the back wall may also be observed in our simulations and is responsible for the separation between the suspension and the left wall. In our simulations, the bore appears to travel somewhat faster than in the corresponding experiments. The difference in bore velocity is likely due to our assumption of a no-slip top boundary rather than a free surface. Our model therefore does not accurately reproduce the effects of the light fluid backflow. However, with the exception of the progression of the bore, the main features of the particle driven current are adequately captured by our model and we therefore expect than in a deep ambient, where no bore is present, our model would describe particle-laden currents more accurately, as was the case for density currents. It should be noted that in the experiments, the bottom surface was a solid wall and we therefore prevented any resuspension below the original level of the bottom wall in our simulations.

[28] We compare in Figure 6 the deposit resulting from a particle-driven current to that obtained via our simulations. Here the experimental results of *De Rooij and Dalziel* [2001] are compared to a computed deposit for a current with corresponding parameters. Our simulations again make use of a reduced Reynolds number (2,200 compared to 10,000 in the experiment) and are purely 2-D while the experiments were conducted in a channel of width comparable to its height. The results are seen to be in fairly good agreement as to the extent and elevation of the deposit. Differences are largest near the left hand wall and are probably attributable to variations in the initial conditions: in the experiments particles are kept in suspension by continuous stirring before the lock is released while in our simulations the suspension is initially quiescent. Our simulations are also seen to yield more local variations in the deposit height. Such oscillations result from eddies generated at the top of the current by the strong fluid backflow present in a shallow ambient. Once again, the top surface was free in the experiments, which acts to reduce the shear and thus the formation of stationary eddies. It should be pointed out that a similar comparison was presented by *Necker et al.* [2002]. Their simulations were based on similar equations but did not include resuspension or slope variations. Both set of simulations agree with the experiments because resuspension was in fact negligible in the experimental results of DeRooij and Dalziel [2001]. Note also that *Necker et al.* [2002] also looked at deposits obtained via 3-D simulations and found negligible differences with those computed with a 2-D code.

[29] Unfortunately, lock-release experiments in which resuspension plays a significant role to our knowledge have not yet been published in the literature. In order to generate sufficiently large current velocities, experiments have only been performed with a constant inflow of particle-laden fluid [*García and Parker*, 1993]. At the present time, our model remains constrained to finite volumes of heavy fluid and we may not compare directly our simulations to experiments where resuspension was significant. However, it may be seen that the size and density ($\bar{d} \sim 100$ μm, $\bar{\rho}_p \sim 2.5$ g/cm^3) of particles subject to re-entrainment at slope angles of order 5° for a current of typical velocity ($\sim$1 m/s) in our simulations are commensurate with available experimental data [*García and Parker*, 1993; *García*, 1994].

[30] The main discrepancies between experiments and simulations therefore result from either initial or top surface conditions. True turbidity currents typically occur in deep ambients so that the effect of the free surface above are inconsequential. We investigate the influence of the height of the computational domain in the next section. The initial velocity of the suspension also differ between experiments and simulations, and is vastly unknown for real turbidity currents. However, the discrepancies resulting from such variations in initial conditions are short-lived. We are here concerned with the development of the current at intermediate times, where comparisons with experiments

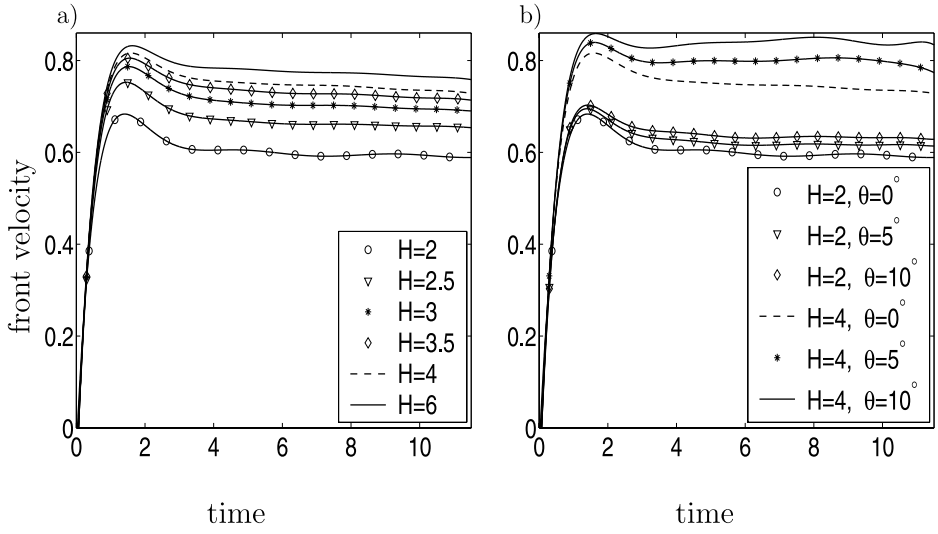

Figure 7. (a) Time dependence of the front velocity, u_f, for different values of the computational domain height, H for a fixed initial heavy fluid height of 2. The dependence of the front velocity on H is relatively weak for $H \geq 4$. (b) Time dependence of the front velocity for different inclination angles θ for both shallow, $H = 2$, and deep, $H = 4$, ambients. In these simulations we consider density currents ($U_s = 0$) propagating over a horizontal surface with $Re_T = Pe_T = 2{,}200$ and initial length $x_f = 2$.

show that our model adequately describes the dynamics of the particle-laden gravity currents.

3.3. Effect of the Computational Domain Height

[31] We now investigate the influence of the computational domain height, H, on the propagation velocity of the current. Experiments show that light fluid back flow may significantly reduce the velocity of currents spreading in shallow surroundings [*Huppert and Simpson*, 1980]. Figure 7a shows the progression of the nose of density currents ($U_s = 0$), defined as the furthest point in the x_1 direction where $C > 0.5$, traveling over a flat surface for different values of H. After a brief acceleration period, the velocity of the current's front remains nearly constant over the first 20 nondimensional time units. At longer times, the current decelerates slowly as the height of its head decreases. Currents traveling in deep ambient fluid are not readily affected by the fluid back flow and thus travel faster downstream. Such currents also shed significantly fewer vortices, and therefore dissipate much less energy through viscous effects. It may be seen from Figure 7a that computations performed with $H \geq 4$ are not significantly influ-

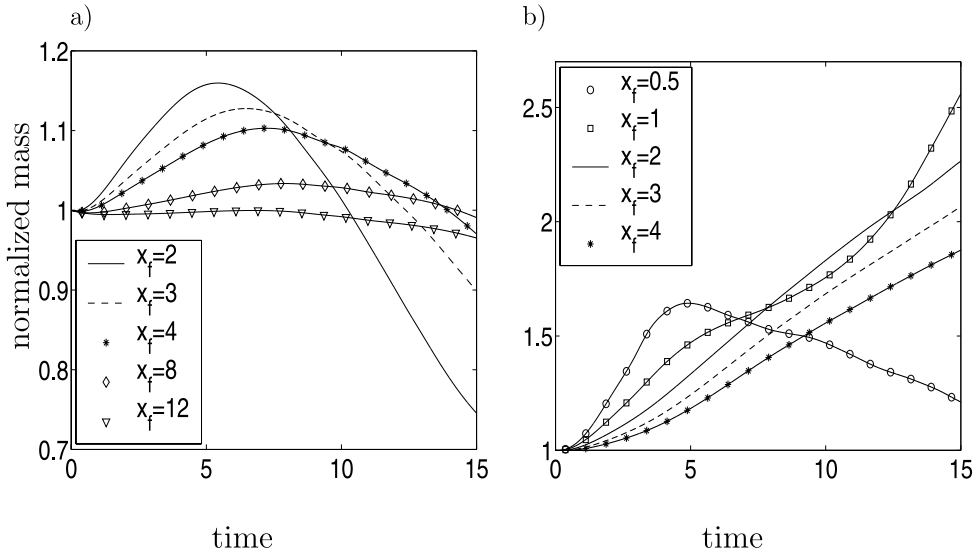

Figure 8. Time dependence of the current mass normalized by the initial mass for various initial length, x_f, at two different inclination angles, (a) $\theta = 3°$ and (b) $\theta = 4°$. Provided that $x_f \geq 1$, the long-term behavior of the current appears to be independent of the precise value of x_f. In these simulations we consider deep-water particle-laden currents, $H = 4$, with $U_s = 0.02$, $Re_p = 3.83$, and $Re_T = Pe_T = 2{,}200$.

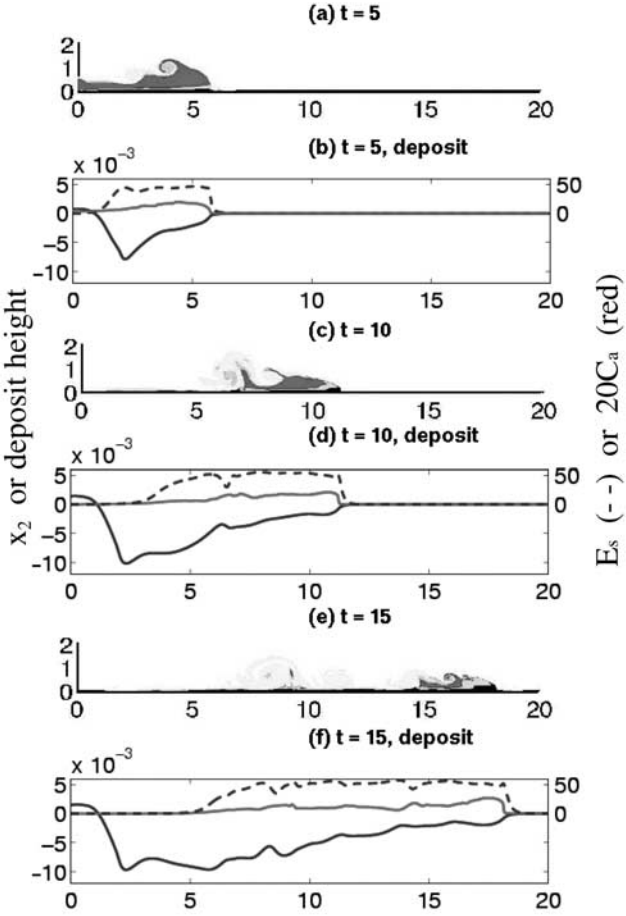

Figure 9. (a, c, and e) Evolution of the particle concentration and (b, d, and f) evolution of the bed height, resuspension factor E_s, and average concentration $C_a = \int_0^H C dz$, multiplied by 20 for scaling purposes (red lines), of a strongly resuspending gravity current. The color code is: $0.1 < C \leq 0.5$ yellow, $0.5 < C \leq 0.8$ green, $0.8 < C \leq 1$ red, $1 < C \leq 3$ cyan, and $3 < C$ black. In Figures 9b, 9d, and 9f the left scale refers to the bed height (solid lines), and the right scale to E_s (dashed lines) and 20 C_a (red lines). Other parameters are $\theta = 5°$, $\bar{d} = 100$ μm, $\bar{h} = 1.6$ m, $\bar{C}_0 = 0.5\%$, $U_s = 0.02$, $Re_T = Pe_T = 2{,}200$, $x_f = 2$, and $H = 4$. See color version of this figure at back of this issue.

enced by the precise value of H and thus may be used to simulate gravity currents in very deep surroundings.

[32] Figure 7b shows the front velocity, u_f, of density currents propagating on slopes of constant angles in both shallow ($H = 2$) and deep ($H = 4$) computational domains. In a deep ambient the front velocity is known experimentally to increase slightly with slope angle both for constant flux [*Britter and Linden*, 1980] and constant initial volume [*Beghin et al.*, 1981]. Our simulations reveal a similar dependence of u_f on the slope angle. After an initial slumping phase, the currents travel at nearly constant speed, $u_f = 0.77$ for $\theta = 0°$, $u_f = 0.80$ for $\theta = 5°$ and $u_f = 0.83$ for $\theta = 10°$, showing a nearly linear dependence of the front velocity on θ. Significant mixing between the current and the ambient fluid is observed for large slope angles, reducing the velocity at later times as the size of the head decreases. In a shallow ambient, the slope angle has a negligible impact on the propagation velocity of the current (Figure 7b). Irrespectively of the slope angle, lighter fluid back flow hinders the progression of the current and generates numerous energy dissipating vortices.

3.4. Influence of the Initial Current Length

[33] For resuspending currents, the time evolution of the mass of suspended particles is of primary importance in the description of the flow. If the mass of the currents increases in time, currents which we refer to as self-sustaining, the flow is mostly eroding and may travel for very large distances provided that the inclination angle remains sufficiently large. In contrast, currents traveling along relatively flat surfaces see their mass decrease in time and are mostly depositional. These currents quickly stop spreading as particles are deposited.

[34] We proceed to investigate the influence of the initial current length, x_f, on the time evolution of gravity currents and in particular on their self-sustaining quality. Figure 8a shows the time dependence of the mass of suspended particles of currents propagating over a small inclination angle, $\theta = 3°$, such that a current with $x_f = 2$ is depositional. Here the initial mass is normalized to one. The mass of suspended particles first increases briefly during the slumping phase of the current. However, at later times, the settling of particles exceeds resuspension and the total mass decreases. Increasing the initial length is seen to have no qualitative impact on the time dependence of the mass. The initial normalized mass increase is less for longer currents since the amount of resuspended particles near the front is nearly independent of x_f.

[35] For a larger slope angle, $\theta = 4°$, a current with $x_f \geq 1$ becomes self-sustaining and its mass increases with time, see Figure 8b. Once again, the relative mass increase is smaller for longer currents. Notice that very short and tall currents, e.g., with $x_f = 0.5$ behave in a qualitatively different manner and appear mostly depositional. The initial length of the current therefore has little impact on whether or not the current will become self-sustaining, provided it is larger than a critical value near $x_f = 1$. In the remainder of the simulations presented here, we thus fix the initial current length equal to its initial height at $x_f = 2$.

3.5. Influence of Resuspension

[36] Figure 9 shows an example of a strongly resuspending current. Here the slope angle is sufficiently large, $\theta = 5°$, and the particle settling speed sufficiently small, $U_s = 0.02$, so that the amount of resuspended particles exceeds that of deposited particles. Unresolved turbulent motions, modeled as a diffusive effect, are responsible for the high concentration observed below $x_2 \approx 0.1$, while the increase in particle concentration at higher levels is mostly attributable to the advection of the concentration through resolved fluid motions. As the current propagates downslope, its mass and velocity increase. In our system, the only saturation mechanism is the resuspension upper bound $E_s \leq 0.3/\bar{C}_0$, so the current may grow until the average particle concentration reaches a level where the average particle-particle interactions may not be neglected ($\bar{C} \sim 10\%$) and our model no longer applies.

[37] In the early stages of motion (Figure 9a), the current resembles a noneroding gravity current and only a small

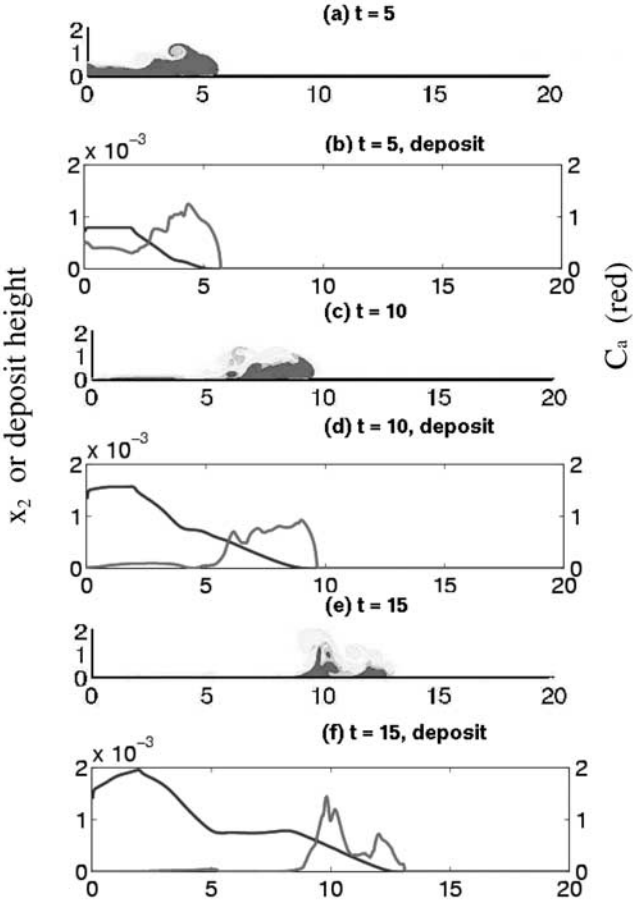

Figure 10. (a, c, and e) Evolution of the particle concentration and (b, d, and f) evolution of bed height (blue lines) and average concentration $C_a = \int_0^H C dz$ (red lines), of a nonresuspending gravity current at times $t = 5$ (Figures 10a and 10b), 10 (Figures 10c and 10d) and 15 (Figures 10e and 10f). The color code is $0.1 < C \leq 0.5$ yellow, $0.5 < C \leq 0.8$ green, and $0.8 < C \leq 1$ red. The flow parameters are as in Figure 9: $\theta = 5°$, $\bar{d} = 100$ μm, $\bar{h} = 1.6$ m, $\bar{C}_0 = 0.5\%$, $U_s = 0.02$, $Re_T = Pe_T = 2{,}200$, $x_f = 2$, and $H = 4$, but the resuspension factor E_s has been set to 0. See color version of this figure at back of this issue.

boundary layer at the bottom exhibits a larger particle concentration than $\bar{C}_0$. For comparison, we have included in Figure 10a an example of a current where the flow parameters are identical but resuspension is not taken into account ($E_s = 0$). In both cases, mixing with clear fluid dilutes the upper part of the current and the vortices shed behind the front are very similar. In the presence of resuspension, the particle concentration increases near the front and the formation of a massive head is observed (Figures 9c and 9e). The volume of the head does not change significantly as the current progresses, but it becomes denser, as illustrated by the integrated concentration profile, $C_a = \int_0^H C\, dz$, displayed in red in Figures 9b, 9d, and 9f). The head becomes progressively heavier as resuspended particles accumulate near the front and it thus propagates faster, generating further erosion.

[38] In the presence of resuspension, particles are deposited near the left wall, but strongly eroded near the initial front position, $x_f = 2$, as the initial slumping phase generates vigorous erosion (Figure 9b). Further downstream, $x_1 > x_f$, the erosion pattern is mostly flat in regions behind the current and increases nearly linearly toward the position of the nose of the current. The thin boundary layer preceding the bulk of the current indicates that the erosion process may begin ahead of the front of the current as motions in the ambient fluid are sufficiently vigorous to generate resuspension, The magnitude of the resuspension factor remains nearly constant, $E_s \approx 50$, and is close to saturation ($E_s < 0.3/\bar{C}_0 = 60$), in the regions where particle-laden fluid is present. The depth of the eroded region is thus approximately proportional to the time interval during which fluid overlies a given point and depends only weakly on the distance from the source. In the absence of resuspension, see Figures 10b, 10d, and 10f, the deposit may only increase in time. The local height of the deposit reflects the time during which the current overlaid a given point.

3.6. Dependence of Mass and Velocity on Slope Angle

[39] The slope angle, θ, plays a determinant role in the long term behavior of resuspending currents. For sufficiently large values of θ, the resuspended particles contribute significantly to the potential energy of the current and allow the current to become self-sustaining. Figure 11 shows the time evolution of the mass of suspended particles (Figure 11a) and front velocity (Figure 11b) of currents propagating at different slope angles. In the depositional regime ($\theta = 0°$, $\theta = 2°$), the mass of the current quickly decreases and shows little dependence on the slope angle. Similarly, the velocity of the front slowly decreases after a brief acceleration period. As particles settle out of suspension, the driving force is reduced and the front velocity decreases earlier than for a corresponding density current, see Figure 7.

[40] For a larger slope angle ($\theta = 6°$), the mass increases in a nearly exponential fashion while it increases almost linearly for an intermediate angle ($\theta = 4°$). The slope angle is clearly seen to control the rate of increase, with larger slope angles generating significantly larger entrainment rates. Correspondingly, the front velocity increases with slope angle. As the head becomes denser, the pressure difference between the current and the ambient increases, thus giving rise to a larger driving force. For given flow parameters, there exists a critical slope angle, θ_c, above which the mass of the current increases in time and below which all particles eventually settle out. In the next section, we investigate the dependence of the critical angle of various flow parameters.

3.7. Self-Sustainment Criteria

[41] We now wish to characterize the conditions under which a gravity current is self-sustaining. We consider only currents propagating in deep ambients, $H = 4$, and with initial aspect ratio equal to one ($x_f = 2$). We also fix the reduced Péclet and Reynolds numbers, as well as the particle density and the fluid density and viscosity. We focus our attention on the effects of the initial (dimensional) height of heavy fluid, particle concentration and particle radius.

[42] We first note that the particle flux at the lower boundary, $F = (-(\cos\theta)\, C|_{x_2=0} + E_s)\, U_s$, allows to readily distinguish between the influence of the particle settling speed, U_s, and that of the resuspension factor, E_s. We find

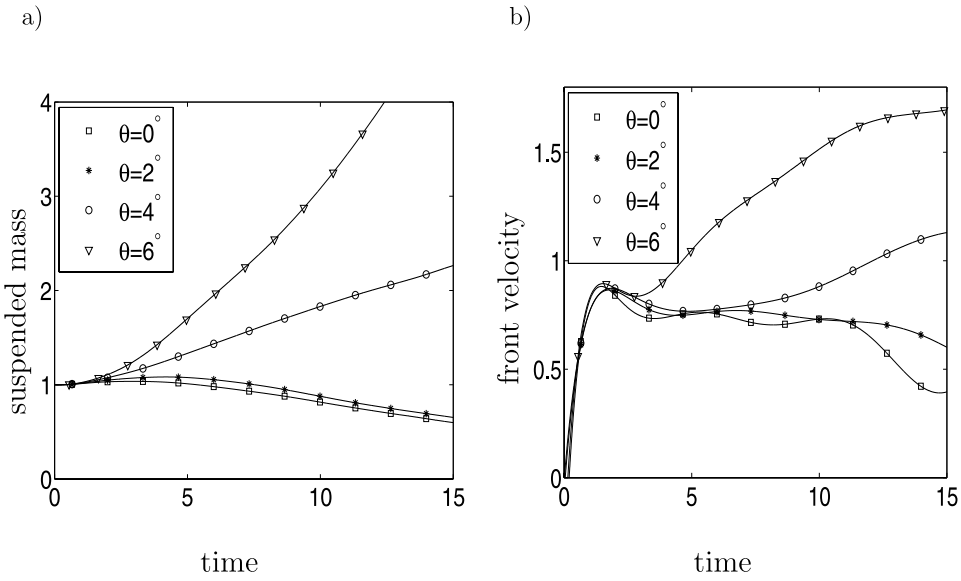

Figure 11. Time dependence of the (a) normalized mass of suspended particles and (b) front velocity of currents propagating over slopes of various slope angle. A critical angle may be found, $\theta_c = 3.75°$, for which $\theta > \theta_c$ gives rise to currents whose mass increases indefinitely and $\theta < \theta_c$ generates depositional currents. Here the flow parameters are $Re_T = Pe_T = 2{,}200$, $x_f = 2$, $H = 4$, $\bar{d} = 100$ μm, $\bar{h} = 1.6$ m, $\bar{C}_0 = 0.5\%$, and $U_s = 0.02$.

that if the resuspension factor is kept constant, the self-sustaining quality of the current is largely unaffected by changes in the particle settling speed. Changes in U_s influence the timescale over which particles settle or are resuspended but do not affect the mass balance directly. However, variations in the particle settling speed typically affect E_s and therefore, through the resuspension factor, influence the critical self-sustaining angle.

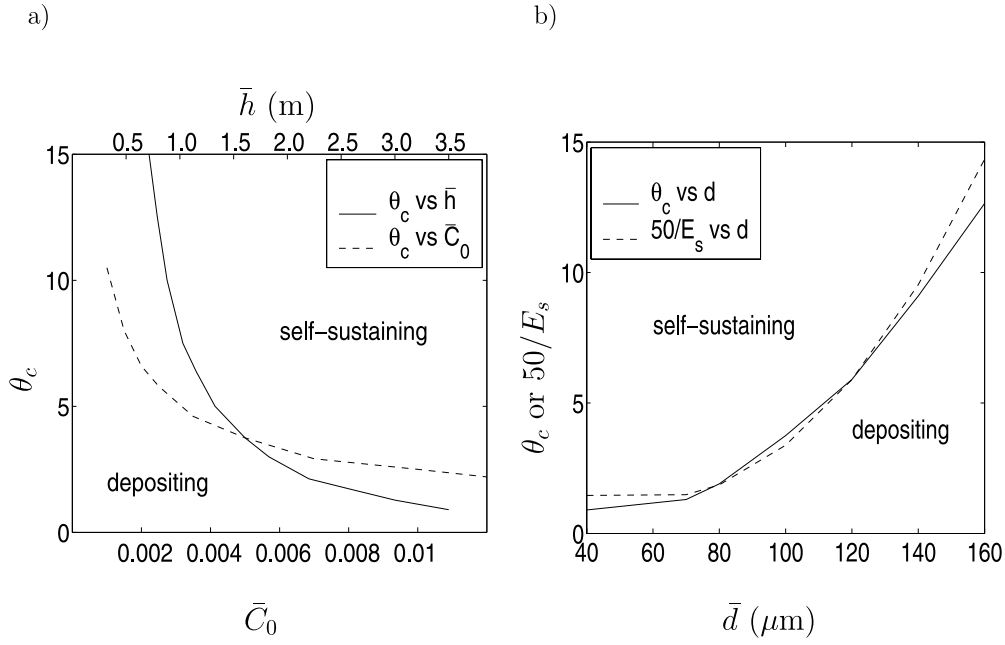

Figure 12. (a) Dependence of the critical self-sustaining angle θ_c on the initial heavy fluid height, $\bar{h}$, (solid line, top scale) and on the initial particle concentration $\bar{C}_0$, (dashed line, bottom scale). (b) Dependence of the critical angle on particle radius (solid line). For comparison we show the dependence of $50/E_s$ on particle radius (dashed line), where E_s is the resuspension factor computed using a typical value of the shear velocity $u^* = 0.13$. Currents located above the curves are self-sustaining, while those located below are depositional. The parameters used in these simulations are $Re_T = Pe_T = 2{,}200$, $x_f = 2$, $H = 4$, $\bar{d} = 100$ μm, $\bar{C}_0 = 0.5\%$, and $\bar{h} = 1.6$ m. Each of the last three parameters is varied individually while keeping the other two fixed at the value mentioned here.

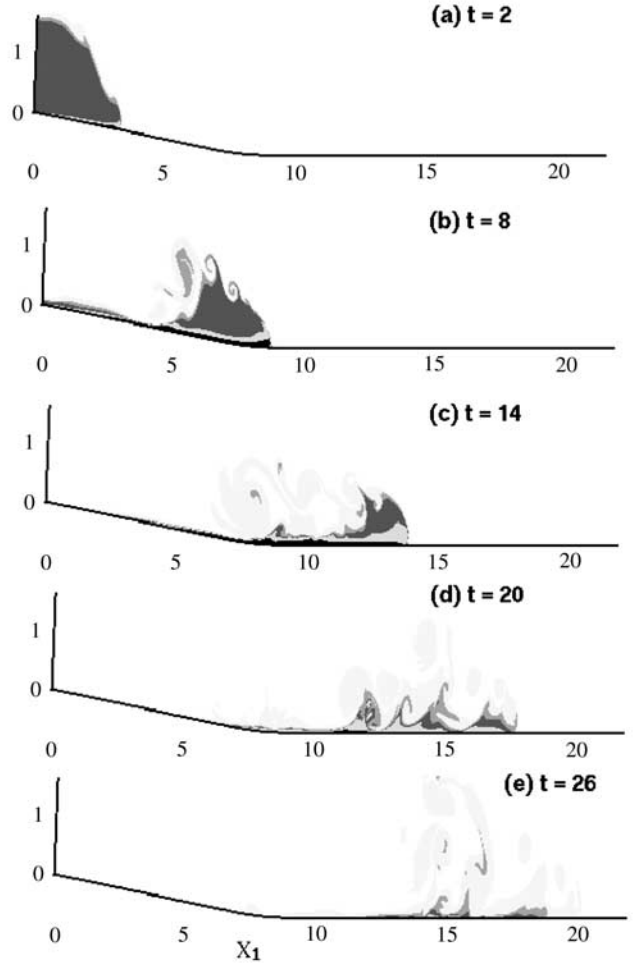

Figure 13. Particle concentration of a resuspending current traveling down a broken slope at times t = 2, 8, 14, 20, and 26. The initial slope angle is $\theta = 5°$, and the angle decreases linearly to 0 in the region $7 \leq x_1 < 9$. Corresponding current mass, velocity, and particle deposits may be found in Figure 14. The color code is: $0.1 < C \leq 0.5$ yellow, $0.5 < C \leq 0.8$ green, $0.8 < C \leq 1$ red, $1 < C \leq 3$ cyan, and $3 < C$ black. The flow parameters are, again, $\bar{d}$ = 100 μm, $\bar{h}$ = 1.6 m, $\bar{C}_0$ = 0.5%, U_s = 0.02, $Re_T = Pe_T$ = 2,200, x_f = 2, and H = 4. See color version of this figure at back of this issue.

[43] We present in Figure 12 the dependence of the critical slope angle θ_c on the heavy fluid height and initial particle concentration in Figure 12a and particle radius in Figure 12b. Here we keep $Re_T = Pe_T$ fixed, but we allow all other parameters to vary. The dimensional settling speed, buoyancy velocity, particle Reynolds number and resuspension factor are computed using the formulas of *Dietrich* [1982] and equations (1), (9) and (10), respectively, with varying values of $\bar{h}$, $\bar{d}$, and $\bar{C}_0$. As expected, large critical slope angles are associated to small values of $\bar{C}_0$ and $\bar{h}$. As either $\bar{C}_0$ or $\bar{h}$ increases, the typical velocity of the current $\bar{u}_b = \sqrt{(g\bar{h}\bar{C}_0 R)}$ increases, and currents may thus generate larger bottom shear stresses. In nondimensional form, as the current velocity increases, the settling speed U_s diminishes, causing E_s to increase. The influence of $\bar{C}_0$ is weaker than that of $\bar{h}$; particle re-entrainment will affect low particle concentration currents more readily as the relative particle concentration will then become larger, thus partially counteracting the fact that low values of $\bar{C}_0$ reduce the current velocity.

[44] Figure 12b shows that increasing the particle radius renders resuspension more difficult since large particle radii cause E_s to decrease. For comparison, we show the dependence on particle size of a typical value of the inverse of the resuspension factor ($50/E_s$, scaled for plotting purposes). Both curves are nearly parallel, indicating that E_s is the determinant factor in the self-sustaining quality of a current. This underlines the importance of accurately determining E_s and in particular the value of Z at which resuspension first becomes important (equation 10), as it will directly influence the value of the critical angle for given flow parameters.

[45] In the parameter regime and for the resuspension factor investigated here, we therefore find, by fitting the curves shown in Figures 12a and 12b to a power law, that currents are self-sustaining if

$$1 < K \frac{\sin\theta_c \left(\bar{h}\bar{C}_0\right)^{5/3}}{\bar{d}^{11/4}\bar{C}_0} \approx \frac{\sin\theta_c}{\sin 3.75°} \frac{\left(\frac{\bar{h}}{1.6\mathrm{m}}\frac{\bar{C}_0}{0.5\%}\right)^{5/3}}{\left(\frac{\bar{C}_0}{0.5\%}\right)\left(\frac{\bar{d}}{10^{-4}\mathrm{m}}\right)^{11/4}} \qquad (11)$$

where K is a constant determined by the critical angle associated with our default parameter values $\bar{d} = 10^{-4}$ m, $\bar{h}$ = 1.6 m and $\bar{C}_0$ = 0.005. Turbidity currents may thus be expected to grow in size as long as the inclination angle of the lower boundary is larger than θ_c, and to decay over regions where $\theta < \theta_c$.

3.8. Broken Slope Currents

[46] We present here an application of our model to turbidity currents traveling down a slope of varying angle. To simulate the base of the continental slope, we selected a geometry where the initial slope is 5° and the surface away from the source is horizontal. The slope remains constant for $x_1 < 7$ and decreases linearly to 0° in the region $7 \leq x_1 < 9$. The current and particle parameters were chosen to cause the mass of the current to increase over the inclined region.

[47] Figure 13 shows the progression of a current traveling down a broken slope. In the early stages of motion, the current is erosional and its concentration increases near the lower boundary. However, upon reaching the horizontal bed, the current becomes depositional and eventually comes to rest. The transition from flow over an incline to flow over a horizontal bottom surface occurs smoothly and no significant changes in the height of the current (hydraulic jump) is observed near the corner. The finite volume of heavy fluid presumably prevents us from observing steady hydraulic jumps such as those reported by *García* [1993].

[48] Figure 14a illustrates the dependence of the mass of suspended particles and front velocity on the position of the current tip. As the current travels downslope, its mass increases through erosion of the bed. The suspended mass continues to increase even after the nose has reached the flat surface, as most of the heavy fluid is still traveling downhill. At later times, all the heavy fluid overlies a horizontal surface and the current becomes depositional, causing the

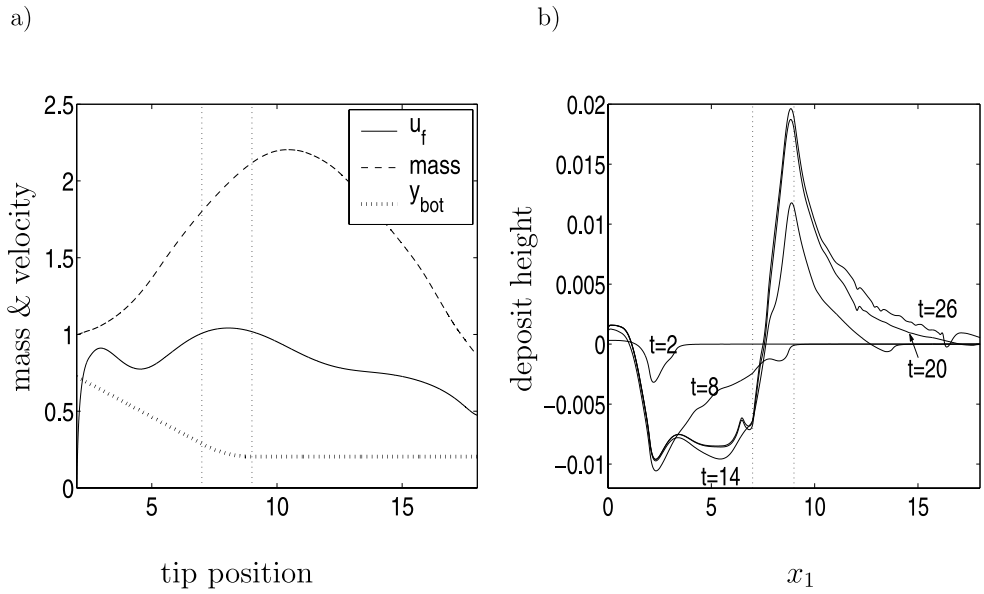

Figure 14. (a) Front velocity (solid line) and suspended mass (dashed line) as a function of the position of the nose of a current propagating over a broken slope. The height of the bottom surface is shown as the dotted line. (b) Dependence of the deposit height on the distance from the left wall at various times for the same current. The region left of the first vertical dotted line has a slope angle of $\theta = 5°$, and that right of the second line one of $\theta = 0°$. Other flow parameters are $Re_T = Pe_T = 2{,}200$, $x_f = 2$, $H = 4$, $\bar{d} = 100$ μm, $\bar{h} = 1.6$ m, $U_s = 0.02$, and $\bar{C}_0 = 0.5\%$.

mass to decrease. The front velocity, after the initial slumping phase, increases while overlying a surface of sufficiently large slope angle. When the nose reaches the corner, the front velocity starts to decrease, showing that the local slope angle readily influences the front velocity. As the current spreads, the velocity keeps decreasing as particles are deposited.

[49] The corresponding deposition pattern is presented in Figure 14b for different times. Particles are deposited near the left wall before the eroding character of the current develops as it moves downstream. The depth of the eroded region remains constant over the region of large slope angle. Near the corner, the current enters a depositional regime and leaves a deposit of maximum height at the beginning of the flat region. The deposit then decreases with distance from the corner. If a current transports sufficient particles, the geometry of the bottom surface may therefore be significantly altered. In particular, the position of the corner is shifted to the left. The cumulative effect of successive turbidity currents could then displace or create large topographic features and have important geological consequences.

4. Conclusion

[50] We have developed a high-resolution simulation model for resuspending turbidity currents traveling over complex bottom topographies. The model allows for predictions of the erosion and deposition rates of interest in geological and industrial processes. Provided the curvature of the bottom surface remains small, the flexibility of the model allows us to consider such problems as how successive gravity currents are influenced by deposits resulting from earlier currents. We may therefore characterize the evolution of large-scale deposit structures, which could eventually be used to locate oil and gas fields hosted by turbidites. In particular, we may simulate the spontaneous formation or damping of local bed topography and the evolution of the overall system topography. Validation information has been presented to support the computational approximations required in order to model realistic flows. It was demonstrated that a reduced Reynolds number Re_T of $O(1000-10{,}000)$ is capable of reproducing many of the flow features observed at much larger physical Reynolds numbers inaccessible to direct numerical simulations [*Parsons and García*, 1998]. The resuspension process is modeled on the basis of the empirical relations determined experimentally by [*García and Parker* [1993], by means of a diffusive flux boundary condition at the top of the particle bed. Here the value of the reduced Péclet number Pe_T was chosen based on the experimental observations by *García* [1994]. In the case of self-sustaining currents, it was seen that the qualitative trends, in particular the dependence of the critical self-sustaining angle on particle size or concentration, are independent of the value of Pe_T.

[51] For strongly resuspending currents, particle-particle interactions may become important. Currents propagating on a slope of large angle were seen to develop regions where the particle concentration exceeds 5%. The viscosity of the suspension [*Huang and García*, 1998], as well as the particle settling speed would then be altered by the presence of neighboring particles [*Richardson and Zaki*, 1954]. Such effects were not included in our simulations, as our main interest was to characterize the onset of self-sustainment,

but they should be incorporated in simulations aiming to describe high particle concentration currents. A second important aspect to incorporate in future research is the polydispersity of the suspended particles, which may have a nontrivial influence on the self-sustaining character of a current. Our model may easily be extended to consider different particle sizes by keeping track of several particle concentrations. The concentration of particles in the bed must also be modeled, since only the topmost particles, the so-called active layer, are available for resuspension [*Parker et al.*, 2000]. Armoring may then occur, where large deposited particles prevent the current from re-entraining smaller underlying particles, which thus prevents further growth of the current [*Karim and Kennedy*, 1986]. Studying the combined effects of polydispersity and repeated flows should lead to a better understanding of the formation of realistic deposits and will therefore be investigated in the near future. Another potentially important aspect of the flow not taken into account in our study is the effect of variations in the spanwise direction. Incorporating such effects requires 3-D simulations, which remain very demanding computationally. However, from a theoretical point of view, our model may be expanded to simulate 3-D flows in a straightforward manner using the approach described by *Necker et al.* [2003] for density currents. Given the appropriate computing resources, one could thus study the formation of 3-D structures such as levees, canyons or mini-basins.

Appendix A: Finite-Difference Formula

[52] We show here as an example, the formula obtained to estimate the first derivative of a function f for non-constant Δx_2

$$af'_{I-1} + f'_i + bf'_{i+1} = \alpha f_{i-2} + \beta f_{i-1} + \gamma f_i + \delta f_{i+1} + \epsilon f_{i+2}, \quad \text{(A1)}$$

where

$$a = \frac{x_{nn}x_p^2x_{pp}}{(x_{nn}-x_n)(x_n+x_p)^2(x_n+x_{pp})},$$

$$b = \frac{-x_n^2x_{nn}x_{pp}}{(x_p-x_{pp})(x_{nn}+x_p)(x_n+x_p)^2},$$

$$\alpha = \frac{-x_n^2x_p^2x_{pp}}{(x_n-x_{nn})^2x_{nn}(x_{nn}+x_p)^2(x_{nn}+x_{pp})},$$

$$\epsilon = \frac{x_n^2x_p^2x_{nn}}{(x_p-x_{pp})^2x_{pp}(x_n+x_{pp})^2(x_{nn}+x_{pp})},$$

$$\beta = x_{nn}x_p^2x_{pp}\left(\frac{6x_n^3 - 2x_{nn}x_px_{pp} - x_n^2(5x_{nn}) + x_n^2(4x_p+5x_{pp}) - x_n(3x_{nn}x_p + 4x_{nn}x_{pp} - 3x_px_{pp})}{x_n(x_n-x_{nn})^2(x_n+x_p)^3(x_n+x_{pp})^2x_n(x_n-x_{nn})^2(x_n+x_p)^3(x_n+x_{pp})^2}\right),$$

$$\delta = x_{nn}x_n^2x_{pp}\left(\frac{-6x_p^3 + 2x_{nn}x_nx_{pp} + x_p^2(5x_{pp}) - x_p^2(4x_n+5x_{nn}) - x_p(3x_{pp}x_n + 4x_{nn}x_{pp} - 3x_nx_{nn})}{x_p(x_p-x_{pp})^2(x_n+x_p)^3(x_{nn}+x_p)^2x_p(x_p-x_{pp})^2(x_n+x_p)^3(x_{nn}+x_p)^2}\right),$$

$$\gamma = \frac{2}{x_n} + \frac{1}{x_{nn}} - \frac{2}{x_p} - \frac{1}{x_{pp}},$$

$$x_p = x_2^{i+1} - x_2^i, \quad x_{pp} = x_2^{i+2} - x_2^i,$$

$$x_{nn} = x_2^i - x_2^{i-2}, \quad x_n = x_2^i - x_2^{i-1}.$$

Similar formulae were obtained for second derivative and approximations near and at the boundary.

[53] **Acknowledgment.** The authors gratefully acknowledge the financial support of BHP Billiton Petroleum.

References

Barenblatt, G. I. (1993), Scaling laws for fully-developed turbulent shear flows. 1. Basic hypotheses and analysis, *J. Fluid Mech.*, *248*, 513–520.

Beghin, P., E. J. Hopfinger, and R. E. Britter (1981), Gravitational convection from instantaneous sources on inclined boundaries, *J. Fluid Mech.*, *107*, 407–422.

Blanchette, F., V. Piche, E. Meiburg, and M. Strauss (2005), Evaluation of a simplified approach simulating gravity currents over slopes of varying angles, *Comput. Fluids*, in press.

Bonnecaze, R. T., H. E. Huppert, and J. R. Lister (1993), Particle-driven gravity currents, *J. Fluid Mech.*, *250*, 339–369.

Bosse, T., L. Kleiser, C. Härtel, and E. Meiburg (2005), Numerical simulation of finite Reynolds number suspension drops settling under gravity, *Phys. Fluids*, *17*(3), 037101.

Britter, R. E., and P. F. Linden (1980), The motion of the front of a gravity current traveling down an incline, *J. Fluid Mech.*, *99*, 531–543.

Choi, S. U., and M. H. García (2002), K-ϵ turbulence modeling of density currents developing two dimensionally on a slope, *J. Hydrol. Eng.*, *128*, 55–63.

Choi, H. G., and D. D. Joseph (2001), Fluidization by lift of 300 circular particles in plane Poiseuille flow by direct numerical simulation, *J. Fluid Mech.*, *438*, 101–128.

de Rooij, F., and S. B. Dalziel (2001), Time and space resolved measurements of deposition under turbidity currents, *Spec. Publ. Assoc. Sediment*, *31*, 207–215.

Dietrich, W. E. (1982), Settling velocity of natural particles, *Water Resour. Res.*, *18*(6), 1615–1626.

Elghobashi, S. E., and T. W. Abouarab (1983), A two-equation turbulence model for two-phase flows, *Phys. Fluids*, *26*(4), 931–938.

Fletcher, C. A. J. (1991), *Computational Techniques for Fluid Dynamics*, vol. 2, 2nd ed., Springer, New York.

García, M. H. (1993), Hydraulic jumps in sediment-driven bottom currents, *J. Hydrol. Eng.*, *119*(10), 1094–1117.

García, M. H. (1994), Depositional turbidity currents laden with poorly sorted sediment, *J. Hydrol. Eng.*, *120*(11), 1240–1263.

García, M. H., and G. Parker (1991), Entrainment of bed sediment into suspension, *J. Hydrol. Eng.*, *117*(4).

García, M. H., and G. Parker (1993), Experiments on the entrainment of sediment into suspension by a dense bottom current, *J. Geophys. Res.*, *98*, 4793–4807.

Hagatun, K., and K. J. Eidsvik (1986), Oscillating turbulent boundary-layer with suspended sediments, *J. Geophys. Res.*, *91*, 3045–3055.

Härtel, C., E. Meiburg, and F. Necker (2000), Analysis and direct numerical simulation of the flow at a gravity current head. Part 1. Flow topology and front speed for slip and no-slip boundaries, *J. Fluid Mech.*, *418*, 189–212.

Hay, A. E., R. W. Burling, and J. W. Murray (1982), Remote acoustic detection of a turbidity current surge, *Science*, *217*, 833–835.

Heezen, B. C., and M. Ewing (1952), Turbidity currents and submarine slumps, and the 1929 Grand-Banks earthquake, *Am. J. Sci.*, *250*(12), 849–873.

Hodson, M. E. (1998), The origin of igneous layering in the Nunarssuit Syenite, south Greenland, *Min. Mag.*, *62*(1), 9–27.

Hogg, A. J., M. Ungarish, and H. E. Huppert (2000), Particle-driven gravity currents: Asymptotics and box-model solutions, *Eur. J. Mech. B Fluids*, *19*, 139–165.

Hsu, T., J. T. Jenkins, and P. L.-F. Liu (2003), On two-phase sediment transport: Dilute flow, *J. Geophys. Res.*, *108*(C3), 3057, doi:10.1029/2001JC001276.

Huang, X., and M. H. García (1998), A Herschel-Bulkley model for mud flow down a slope, *J. Fluid Mech.*, *374*, 305–333.

Hughes-Clarke, J. E., A. N. Shor, D. J. W. Piper, and L. A. Mayer (1990), Large–scale current-induced erosion and deposition in the path of the 1929 Grand Banks turbidity current, *Sedimentology*, *37*, 613–629.

Huppert, H. E., and J. E. Simpson (1980), The slumping of gravity currents, *J. Fluid Mech.*, *99*, 785–799.

Hutter, K. (1996), Avalanches, in *Hydrology of Disasters*, edited by V. P. Singh, chap. 11, pp. 317–393, Springer, New York.

Karim, M. F., and J. F. Kennedy (1986), Degradation of graded-material beds in sediment-deficient rivers, *Int. J. Sediment. Res.*, *1*, 39–55.

Krause, D. C., W. C. White, D. J. W. Piper, and B. C. Heezen (1970), Turbidity currents and cable breaks in the Western New Britain trench, *Geol. Soc. Am. Bull.*, *81*, 2153–2160.

Lele, S. K. (1992), Compact finite difference schemes with spectral-like resolution, *J. Comput. Phys.*, *103*, 16–42.

Necker, F., C. Härtel, L. Kleiser, and E. Meiburg (2002), High-resolution simulations of particle-driven gravity currents, *Int. J. Multiphase Flow*, *28*, 279–300.

Necker, F., C. Härtel, L. Kleiser, and E. Meiburg (2003), Mixing and dissipation in particle-driven gravity currents, *J. Fluid Mech.*, in press.

Normark, W. R., H. Posamentier, and E. Mutti (1993), Turbidite systems: State of the art and future directions, *Rev. Geophys.*, *31*, 91–116.

Pantin, H. M. (1991), A model for ignitive autosuspension in brackish underflows, in *Proceedings of the Euromech 262 Colloquium on Sand Transport in Rivers*, *Estuaries and the Sea*, pp. 283–290, A. A. Balkema, Brookfield, Vt.

Pantin, H. M. (2001), In sediment transport and deposition by particulate gravity currents, *IAS Spec. Publ. 31*, Int. Assoc. Sedimentol.

Parker, G., Y. Fukushima, and H. Pantin (1986), Self-accelerating turbidity currents, *J. Fluid Mech.*, *171*, 145–181.

Parker, G., M. H. García, Y. Fukushima, and W. Yu (1987), Experiments on turbidity currents over an erodible bed, *J. Hydrol. Res.*, *25*, 191–244.

Parker, G., C. Paola, and S. Leclair (2000), Probabilistic Exner sediment continuity equation for mixtures with no active layer, *J. Hydrol. Eng.*, *126*, 818–826.

Parsons, J. D., and M. H. García (1998), Similarity of gravity current fronts, *Phys. Fluids*, *10*, 3209–3213.

Patankar, N. A., T. Ko, H. G. Choi, and D. D. Joseph (2001), A correlation for the lift-off of many particles in plane Poiseuille flows of Newtonian fluids, *J. Fluid Mech.*, *445*, 55–76.

Pratson, L. F., and B. J. Coakley (1996), A model for the headward erosion of submarine canyons induced by downslope-eroding sediment flows., *Geol. Soc. Am. Bull.*, *108*, 225–234.

Richardson, J. F., and W. N. Zaki (1954), Sedimentation and fluidisation: Part I, *Trans. Inst. Chem. Eng.*, *32*, 35–53.

Shraiman, B. I., and E. D. Siggia (2000), Scalar turbulence, *Nature*, *405*, 639–646.

Simpson, J. E. (1997), *Gravity Currents in the Environment and the Laboratory*, 2nd ed., Cambridge Univ. Press, New York.

Smith, J. D., and S. R. McLean (1977), Spatially averaged flow over a wavy surface, *J. Geophys. Res.*, *82*, 1735–1746.

Sparks, R. S. J., S. N. Carey, and H. Sigurdsson (1991), Sedimentation from gravity currents generated by turbulent plumes, *Sedimentology*, *38*, 839–856.

Speziale, C. G. (1991), Analytical methods for the developement of Reynolds-stress closures in turbulence, *Ann. Rev. Fluid Mech.*, *23*, 107–157.

Spiegel, E. A., and G. Veronis (1960), On the Boussinesq approximation for a compressible fluid, *Astrophys. J.*, *131*, 442–447.

Torquato, S., T. Truskett, and P. G. Debenedetti (2000), Is random close packing of spheres well defined?, *Phys. Rev. Lett.*, *84*, 2064–2067.

Zeng, J. J., D. R. Lowe, D. B. Prior, W. J. Wiseman, and B. D. Bornhold (1991), Flow properties of turbidity currents in Bute inlet, British Columbia, *Sedimentology*, *38*, 965–996.

Zhang, Y. H., and J. M. Reese (2001), Particle-gas turbulence interactions in a kinetic theory approach to granular flows, *Int. J. Mulitphase Flow*, *27*(11), 1945–1964.

F. Blanchette and E. Meiburg, Department of Mechanical and Environmental Engineering, University of California, Santa Barbara, Engineering II, Room 2355, Santa Barbara, CA 93106, USA. (blanchef@uchicago.edu)

M. E. Glinsky, BHP Billiton Petroleum, 1360 Post Oak Boulevard, Suite 150, Houston, TX 77056-3020, USA.

B. Kneller, Department of Geology, Meston Building, King's College, Aberdeen AB24 3UE, UK.

M. Strauss, Physics Department, Nuclear Research Center Negev, P.O. Box 9001, IL-84190, Beer Sheva, Israel. (mstrauss@netvision.net.il)

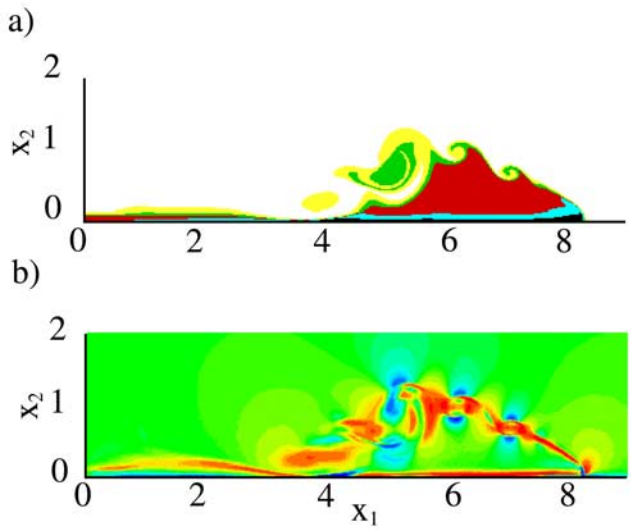

Figure 2. Sample of (a) the concentration and (b) vorticity of a particle-driven current traveling over a surface with an inclination angle $\theta = 5°$, at $t = 7.5$ computed via our numerical model. In Figure 2a the color code is: $0.1 < C \leq 0.5$ yellow, $0.5 < C \leq 0.8$ green, $0.8 < C \leq 1$ red, $1 < C \leq 3$ cyan, and $3 < C$ black. In Figure 2b, positive (counterclockwise), zero, and negative (clockwise) vorticity are shown in red, green, and blue, respectively. The simulation parameters are $H = 4$, $L = 24$, $x_f = 2$, $U_s = 0.02$, $Re_p = 3.83$, and $Re_T = Pe_T = 2{,}200$.

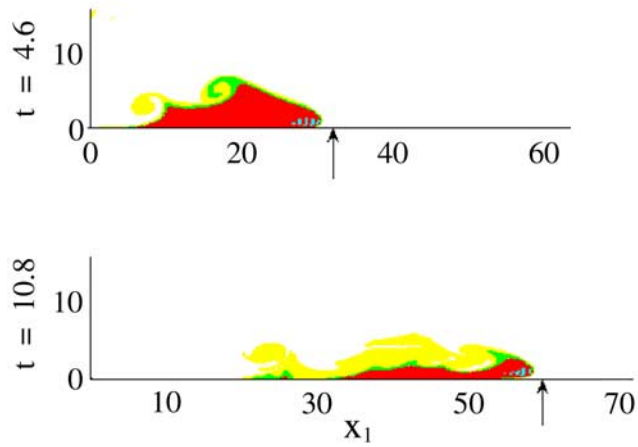

Figure 5. Progression of a particle-laden current with governing parameters identical to those of the current shown in the work of *Bonnecaze et al.* [1993, Figure 9a]. The arrows indicate the position of the front recorded in the experiment. In nondimensional form the parameters used are: $H = 2$, $U_s = 0.03$, $x_f = 1.14$, and $Re_p = 1.8$, and experiments are nondimensionalized using typical length and time $L = 7$ cm and $t = 0.64$ s. The experimental Reynolds number is $Re = 7600$; simulations were performed with a reduced value $Re_T = 2200$.

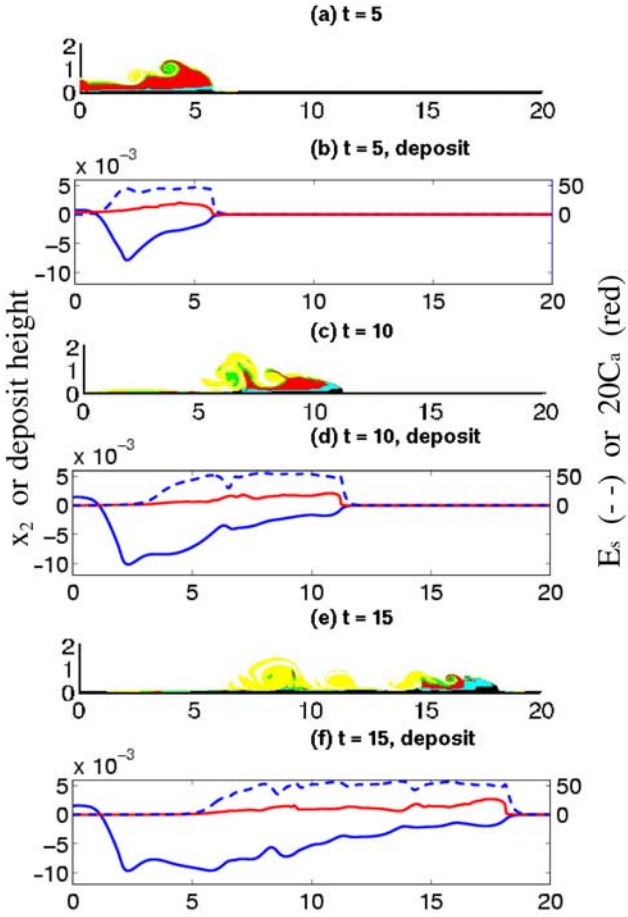

Figure 9. (a, c, and e) Evolution of the particle concentration and (b, d, and f) evolution of the bed height, resuspension factor E_s, and average concentration $C_a = \int_0^H C dz$, multiplied by 20 for scaling purposes (red lines), of a strongly resuspending gravity current. The color code is: $0.1 < C \leq 0.5$ yellow, $0.5 < C \leq 0.8$ green, $0.8 < C \leq 1$ red, $1 < C \leq 3$ cyan, and $3 < C$ black. In Figures 9b, 9d, and 9f the left scale refers to the bed height (solid lines), and the right scale to E_s (dashed lines) and 20 C_a (red lines). Other parameters are $\theta = 5°$, $\bar{d} = 100$ μm, $\bar{h} = 1.6$ m, $\bar{C}_0 = 0.5\%$, $U_s = 0.02$, $Re_T = Pe_T = 2{,}200$, $x_f = 2$, and $H = 4$.

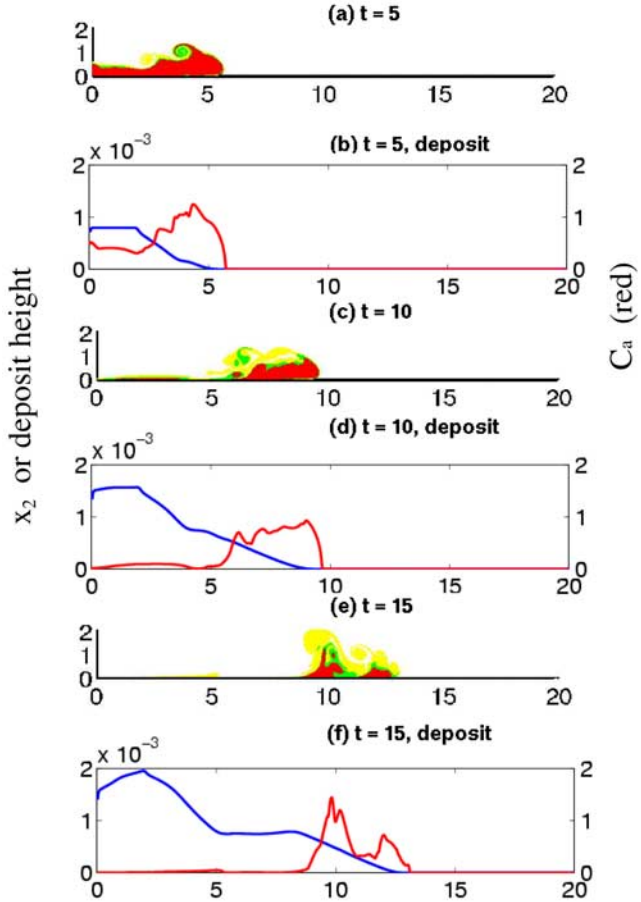

Figure 10. (a, c, and e) Evolution of the particle concentration and (b, d, and f) evolution of bed height (blue lines) and average concentration $C_a = \int_0^H C dz$ (red lines), of a nonresuspending gravity current at times $t = 5$ (Figures 10a and 10b), 10 (Figures 10c and 10d) and 15 (Figures 10e and 10f). The color code is $0.1 < C \leq 0.5$ yellow, $0.5 < C \leq 0.8$ green, and $0.8 < C \leq 1$ red. The flow parameters are as in Figure 9: $\theta = 5°$, $\bar{d} = 100$ μm, $\bar{h} = 1.6$ m, $\bar{C}_0 = 0.5\%$, $U_s = 0.02$, $Re_T = Pe_T = 2{,}200$, $x_f = 2$, and $H = 4$, but the resuspension factor E_s has been set to 0.

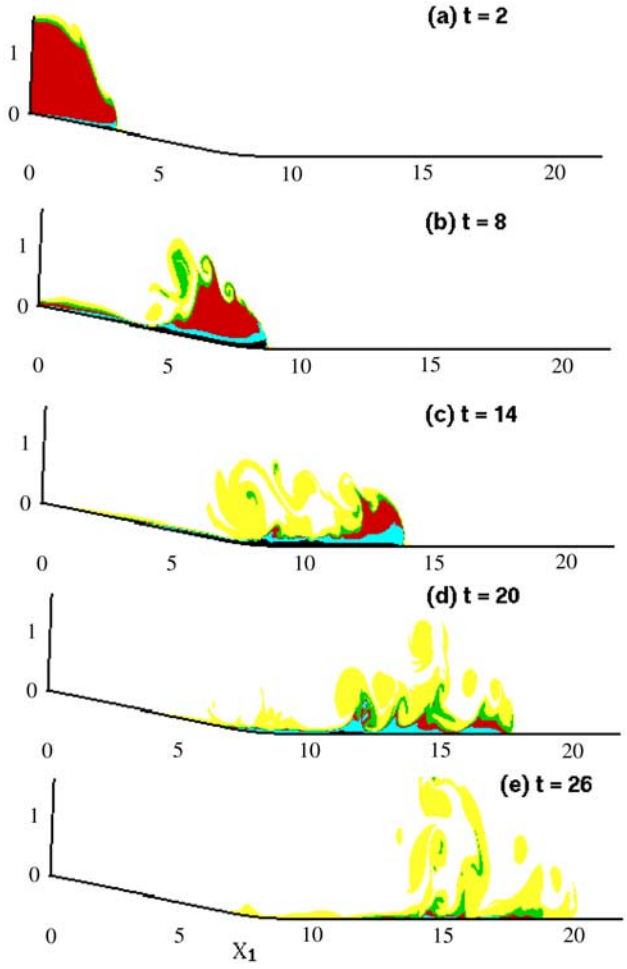

Figure 13. Particle concentration of a resuspending current traveling down a broken slope at times $t = 2$, 8, 14, 20, and 26. The initial slope angle is $\theta = 5°$, and the angle decreases linearly to 0 in the region $7 \leq x_1 < 9$. Corresponding current mass, velocity, and particle deposits may be found in Figure 14. The color code is: $0.1 < C \leq 0.5$ yellow, $0.5 < C \leq 0.8$ green, $0.8 < C \leq 1$ red, $1 < C \leq 3$ cyan, and $3 < C$ black. The flow parameters are, again, $\bar{d} = 100$ μm, $\bar{h} = 1.6$ m, $\bar{C}_0 = 0.5\%$, $U_s = 0.02$, $Re_T = Pe_T = 2{,}200$, $x_f = 2$, and $H = 4$.